Supporting Information

Disentangling anisotropy and exchange in $Co(NCX)_2$ (X = S, Se) chains via THz-EPR spectroscopy

Jooris Beyer[a], Michael Böhme[a], Michał Rams[b], Christian Näther[c] and Winfried Plass[a]

[a] Institut für Anorganische und Analytische Chemie, Friedrich-Schiller-Universität Jena, Humboldtstr. 8, 07743 Jena, Germany; email: sekr.plass@uni-jena.de

[b] Institute of Physics, Jagiellonian University, Łojasiewicza 11, 30348 Kraków, Poland; email: m.rams@uj.edu.pl

[c] Institut für Anorganische Chemie, Christian-Albrechts-Universität zu Kiel, Max-Eyth-Straße 2, 24118 Kiel, Germany; email: cnaether@ac.uni-kiel.de

Contents

Table S1. Selected crystal data and refinement details of the crystal structure determination of **1** and **2**.

	1	**2**
Formula	$C_{12}H_{10}CoN_4Se_2$	$C_{12}H_{10}CoN_4S_2$
MW /g mol^{-1}	427.09	333.29
Crystal system	triclinic	triclinic
Space group	$P\bar{1}$	$P\bar{1}$
a /Å	7.7633(2)	8.5020(2)
b /Å	8.9175(2)	8.6022(2)
c /Å	16.6894(3)	15.5048(3)
α /deg	95.925(2)	93.019(2)
β /deg	97.808(2)	96.374(2)
γ /deg	112.002(2)	114.495(2)
V /Å^3	1046.27(4)	1019.40(4)
T /K	100.0(1)	100.0(1)
Z	3	3
D_{calcd} /g cm^{-3}	2.034	1.629
μ /mm^{-1}	15.534	12.689
$2\theta_{max}$ /deg	161.6	159.1
Refl. collected	12936	9732
Refl. unique	4477	4235
R_{int}	0.0171	0.0296
Refl. [$I > 2\sigma(I)$]	4241	3850
Parameters	259	259
R_1 [$I > 2\sigma(I)$]	0.0327	0.0354
wR_2 (all data)	0.0998	0.1111
GOF	1.099	1.109
$\Delta\rho_{max;\ min}$ /e Å^{-3}	0.89, –0.76	0.55, –0.58

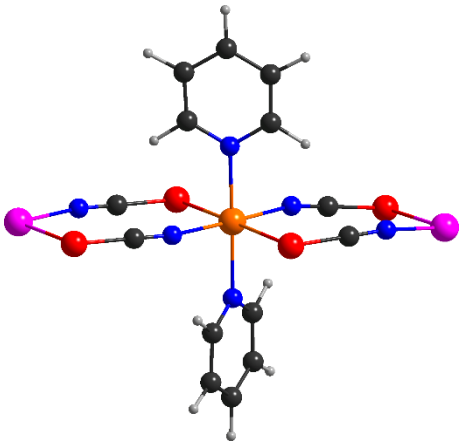

$[CoZn_2(py)_2(NCSe)_4]^{2+}$ (**1**-Co1)

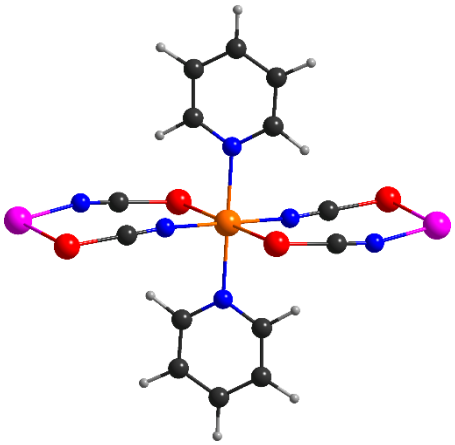

$[CoZn_2(py)_2(NCSe)_4]^{2+}$ (**1**-Co2)

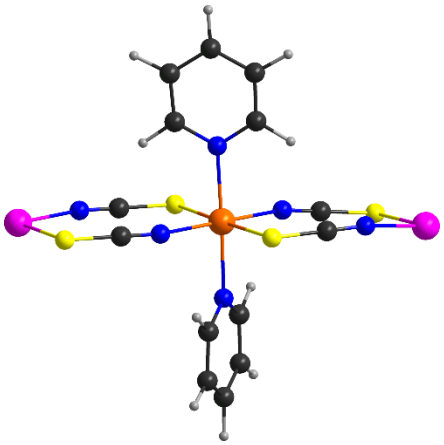

$[CoZn_2(py)_2(NCS)_4]^{2+}$ (**2**-Co1)

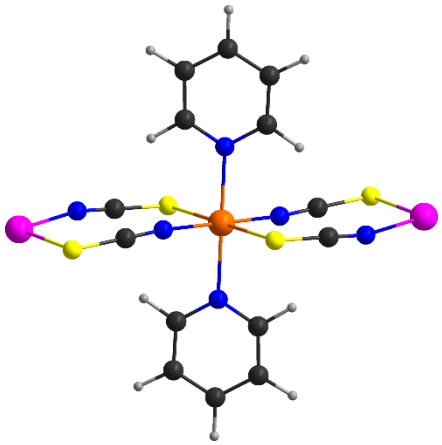

$[CoZn_2(py)_2(NCS)_4]^{2+}$ (**2**-Co2)

Figure S1. Structural models employed for the ab initio calculations of the two crystallographically independent cobalt(II) centers (Co1 and Co2) in **1** (top row) and **2** (bottom row). The pink spheres denote zinc(II) cations introduced to compensate the negative charges of the mononuclear fragments.

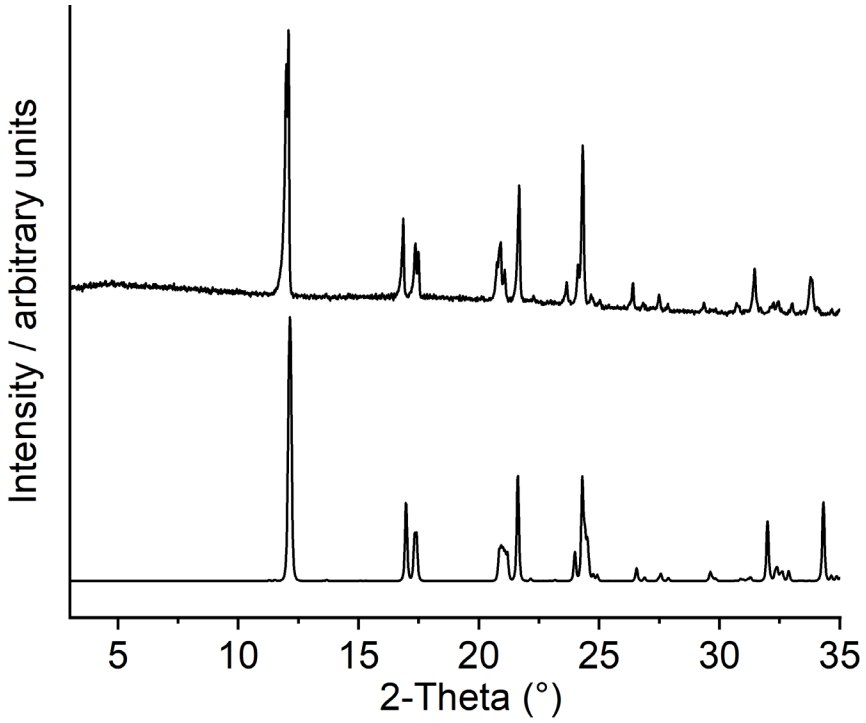

Figure S2. Experimental (top) and calculated (bottom) PXRD pattern for compound **2**.

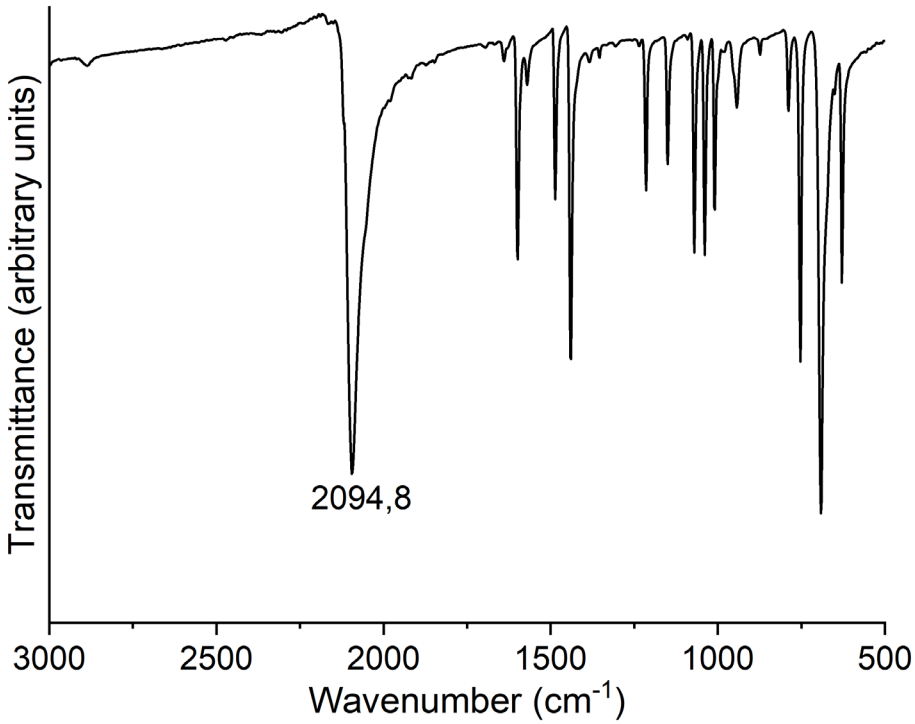

Figure S3. IR spectrum of **2**. Given is the value of the CN stretching vibration of the thiocyanate anions.

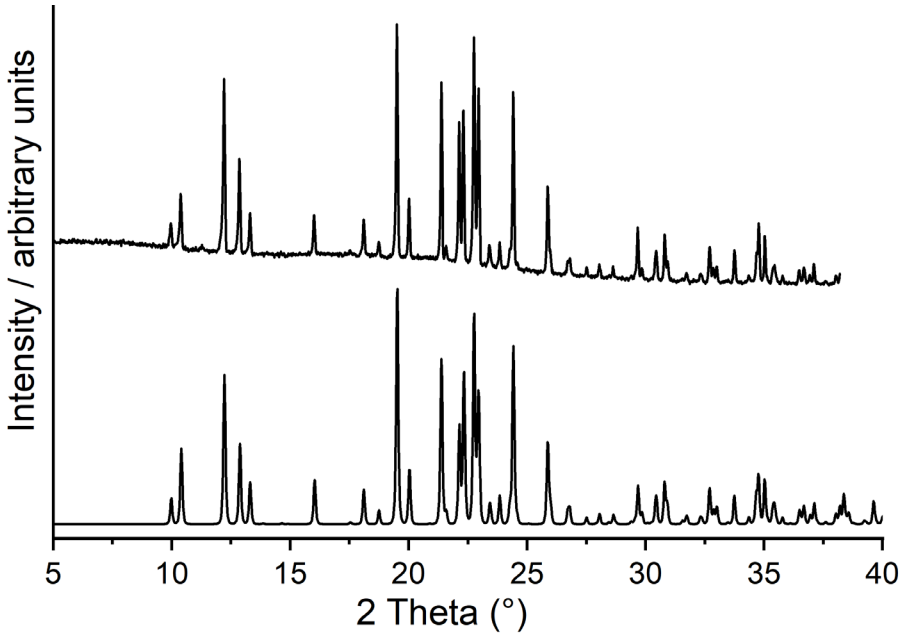

Figure S4. Experimental (top) and calculated (bottom) PXRD pattern for $Co(NCSe)_2(pyridine)_4$.

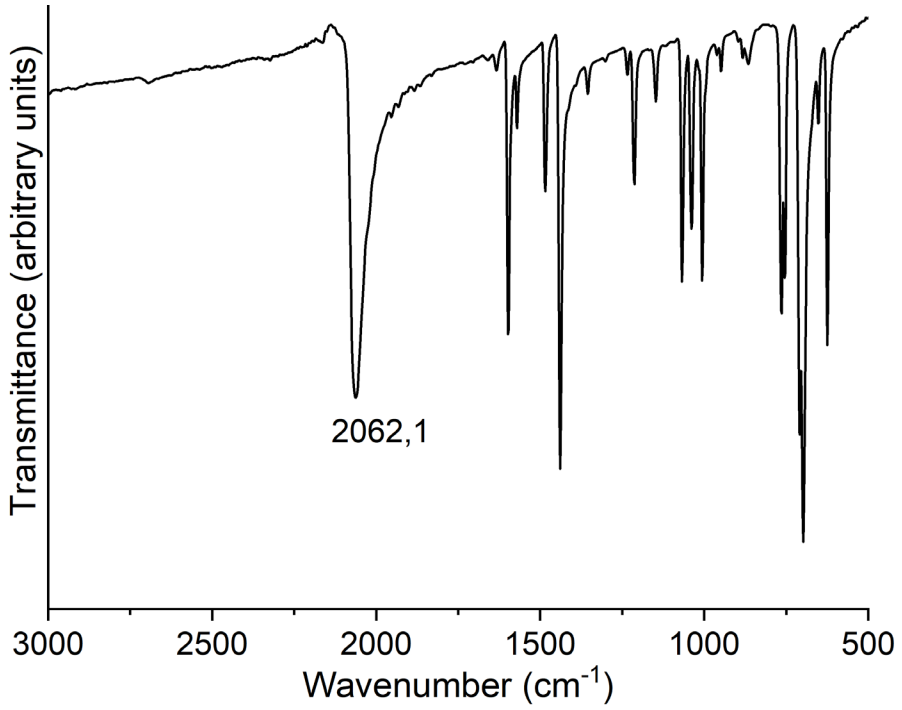

Figure S5. IR spectrum for $Co(NCSe)_2(pyridine)_4$.

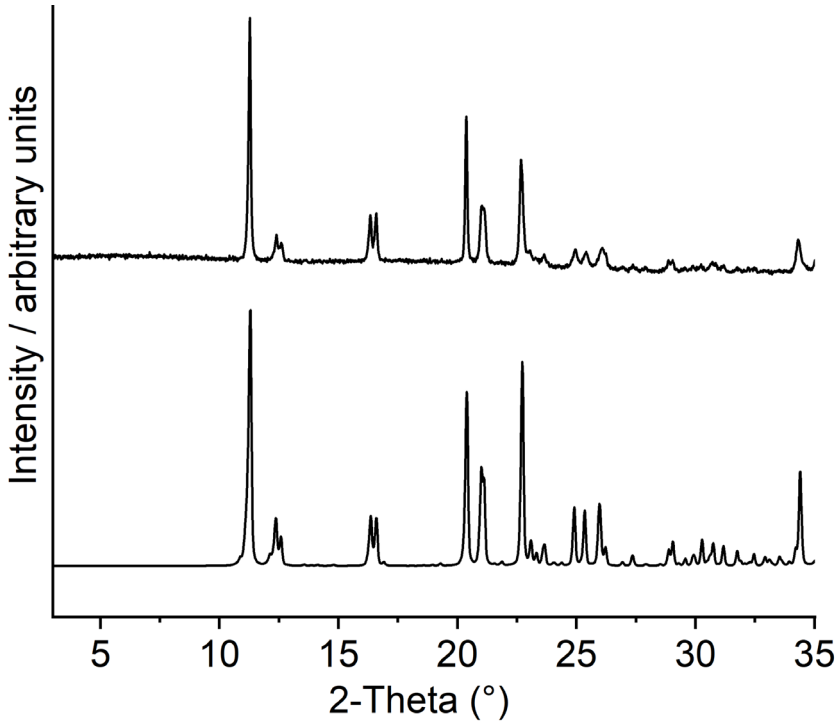

Figure S6. Experimental (top) and calculated (bottom) PXRD pattern for compound **1**. Please note, this compound was obtained after the first mass loss in a thermogravimetric measurement of $Co(NCSe)_2(pyridine)_4$.

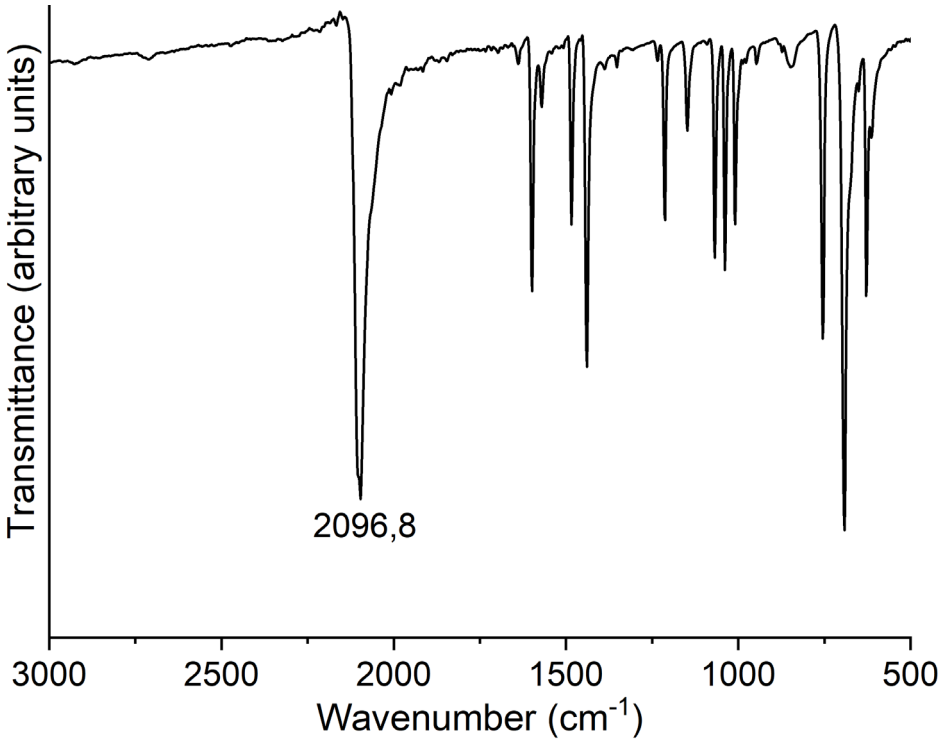

Figure S7. IR spectrum of **1**. Given is the value of the CN stretching vibration of the selenocyanate anions.

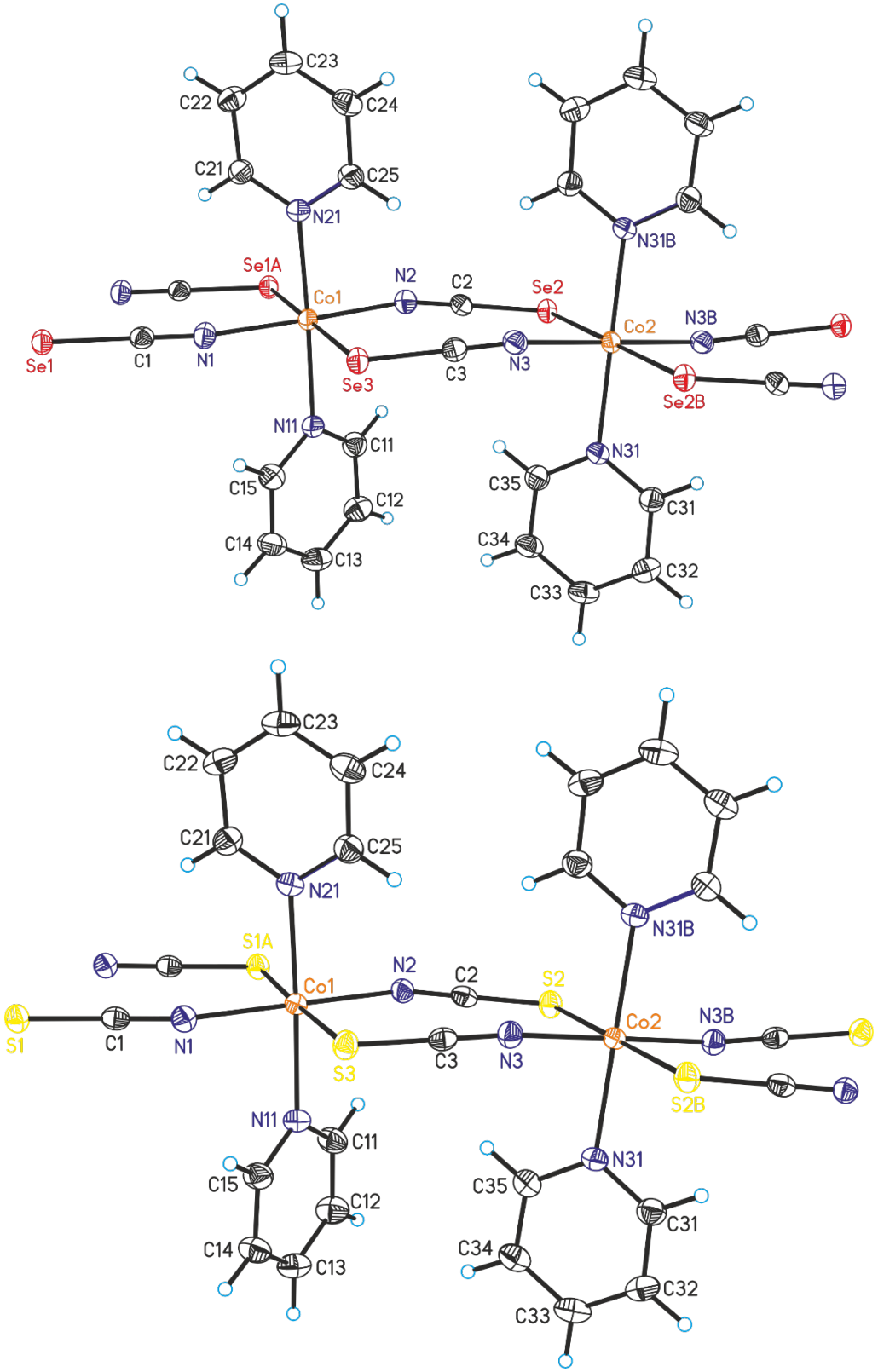

Figure S8. Crystal structure of **1** (top) and **2** (bottom) with labelling and displacement ellipsoids drawn at the 50% probability level. Symmetry codes for the generation of equivalent atoms: A = −x, −y, 1−z; B = −x, 1−y, 2−z.

Table S2. Selected bond lengths (in Å) and angles (in °) for compound **1** and **2**. Symmetry codes for the generation of equivalent atoms: A = −x, −y, 1−z; B = −x, 1−y, 2−z.

Compound **1**				Compound **2**			
Co1	N1		2.057(2)	Co1	N1		2.0562(17)
Co1	Se1A		2.7055(5)	Co1	S1A		2.5807(5)
Co1	N2		2.063(2)	Co1	N2		2.0593(17)
Co1	Se3		2.7149(5)	Co1	S3		2.5881(5)
Co1	N11		2.173(2)	Co1	N11		2.1595(16)
Co1	N21		2.160(2)	Co1	N21		2.1596(16)
Co2	Se2B		2.7365(3)	Co2	S2B		2.6092(5)
Co2	Se2		2.7365(3)	Co2	S2		2.6092(5)
Co2	N3		2.053(2)	Co2	N3		2.0559(17)
Co2	N3B		2.053(2)	Co2	N3B		2.0560(17)
Co2	N31		2.158(2)	Co2	N31		2.1524(16)
Co2	N31B		2.158(2)	Co2	N31B		2.1524(16)
N1	Co1	Se1A	93.86(7)	N1	Co1	S1A	95.10(5)
N1	Co1	N2	178.14(8)	N1	Co1	N2	178.76(5)
N1	Co1	Se3	87.99(7)	N1	Co1	S3	87.30(5)
N1	Co1	N11	89.95(9)	N1	Co1	N11	89.07(7)
N1	Co1	N21	87.60(9)	N1	Co1	N21	88.31(6)
Se1	Co1	Se3	177.402(18)	S1[1]	Co1	S3	177.578(15)
N2	Co1	Se1A	84.58(7)	N2	Co1	S1A	83.87(5)
N2	Co1	Se3	93.61(7)	N2	Co1	S3	93.73(5)
N2	Co1	N11	91.02(9)	N2	Co1	N11	90.24(6)
N2	Co1	N21	91.45(9)	N2	Co1	N21	92.40(6)
N11	Co1	Se1A	88.86(6)	N11	Co1	S1A	90.12(4)
N11	Co1	Se3	89.31(6)	N11	Co1	S3	90.24(4)
N21	Co1	Se1A	92.01(6)	N21	Co1	S1A	90.66(4)
N21	Co1	Se3	89.89(6)	N21	Co1	S3	89.08(4)
N21	Co1	N11	177.45(8)	N21	Co1	N11	177.31(5)
Se2	Co2	Se2B	180.0	S2	Co2	S2B	180.0
N3	Co2	Se2B	93.15(7)	N3	Co2	S2B	86.24(5)
N3	Co2	Se2	93.15(7)	N3	Co2	S2B	93.76(5)
N3	Co2	Se2B	86.85(7)	N3	Co2	S2	93.76(5)
N3	Co2	Se2	86.85(7)	N3	Co2	S2	86.24(5)
N3	Co2	N3	180.0	N3	Co2	N3B	180.00(4)
N3	Co2	N31	89.63(9)	N3	Co2	N31	89.16(6)
N3	Co2	N31B	90.37(9)	N3	Co2	N31B	89.16(6)
N3	Co2	N31B	89.63(9)	N3	Co2	N31B	90.84(6)
N3	Co2	N31	90.37(9)	N3	Co2	N31	90.84(6)
N31	Co2	Se2	90.96(6)	N31	Co2	S2	89.29(4)
N31	Co2	Se2B	90.96(6)	N31	Co2	S2B	89.29(4)
N31	Co2	Se2	89.04(6)	N31	Co2	S2	90.71(4)
N31	Co2	Se2B	89.04(6)	N31	Co2	S2B	90.71(4)
N31	Co2	N31	180.0	N31	Co2	N31[2]	180.0

Table S3. Structure parameters obtained by continuous shape measures for the Co atoms in **1** and **2** for different ideal coordination geometries (OC–6: octahedron; TPR–6: trigonal prism; PPY–6: pentagonal pyramid; JPPY–6: Johnson pentagonal pyramid; HP–6: hexagon)

compound	atom	OC–6 $S(O_h)$	TPR–6 $S(D_{3h})$	PPY–6 $S(C_{5v})$	JPPY–6 $S(C'_{5v})$	HP–6 $S(D_{6h})$
1	Co1	1.611	17.002	28.196	30.631	32.518
	Co2	1.711	17.610	29.132	31.507	32.552
2	Co1	1.141	16.351	28.370	30.931	31.969
	Co2	1.193	17.093	29.014	31.541	32.303

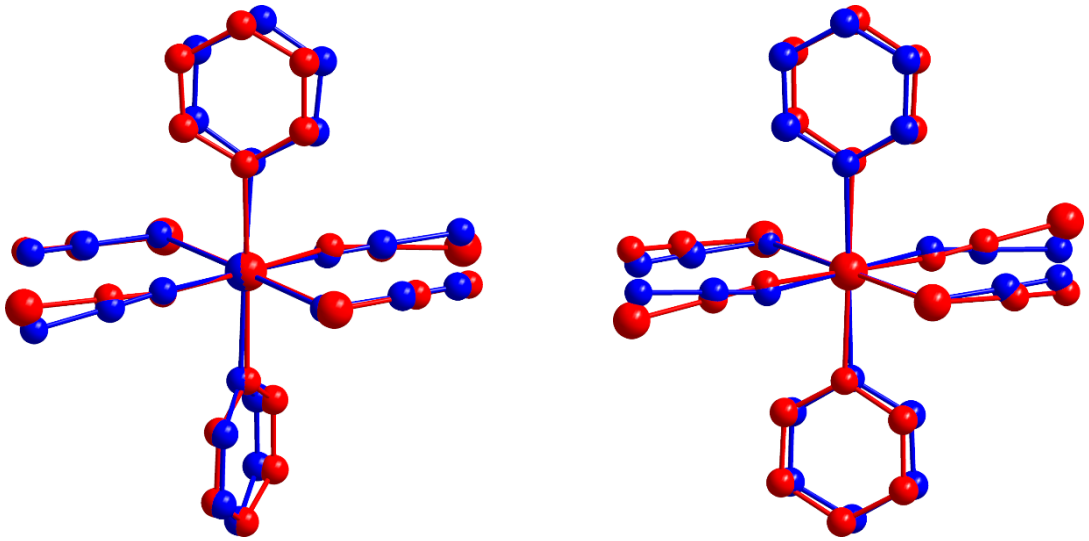

Figure S9. Structural overlay of the coordination sites Co1 (left) and Co2 (right) in **1** (red) and **2** (blue), respectively. Hydrogen atoms have been omitted for clarity.

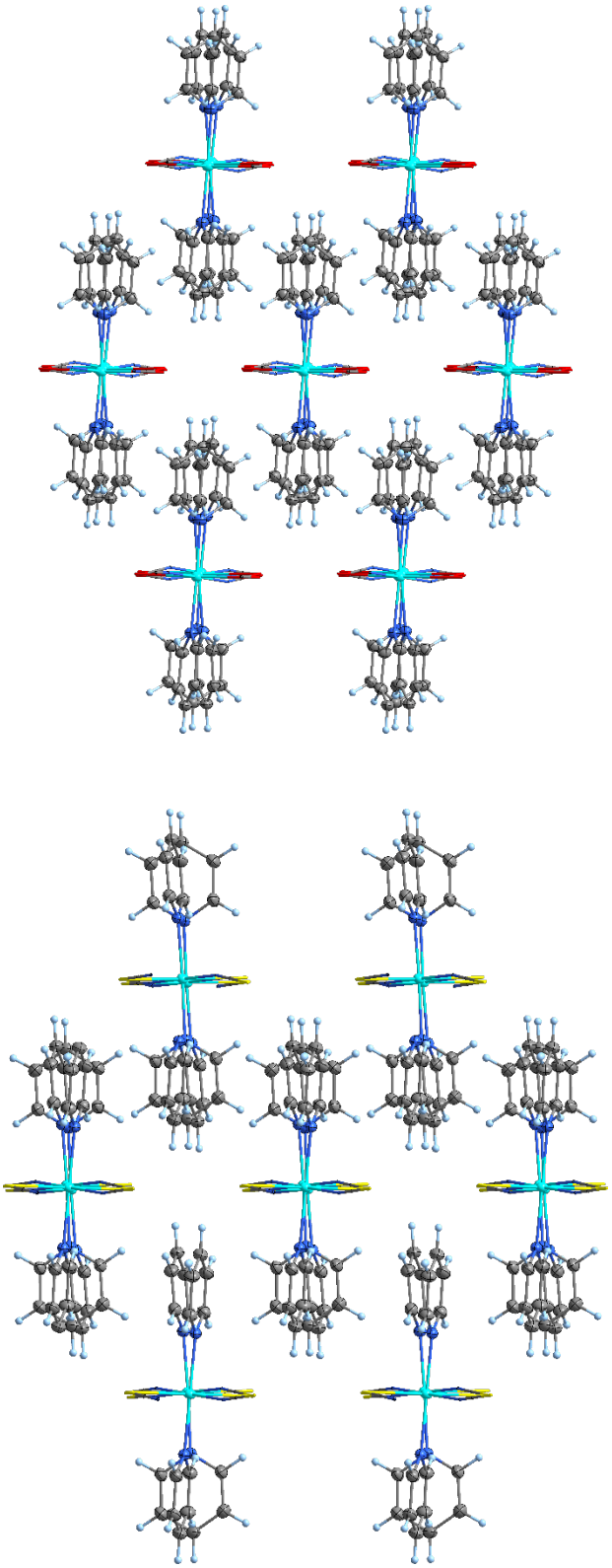

Figure S10. Pseudo-hexagonal arrangement of the chains in compounds **1** (top) and **2** (bottom), viewed along the chain direction in the crystal packing.

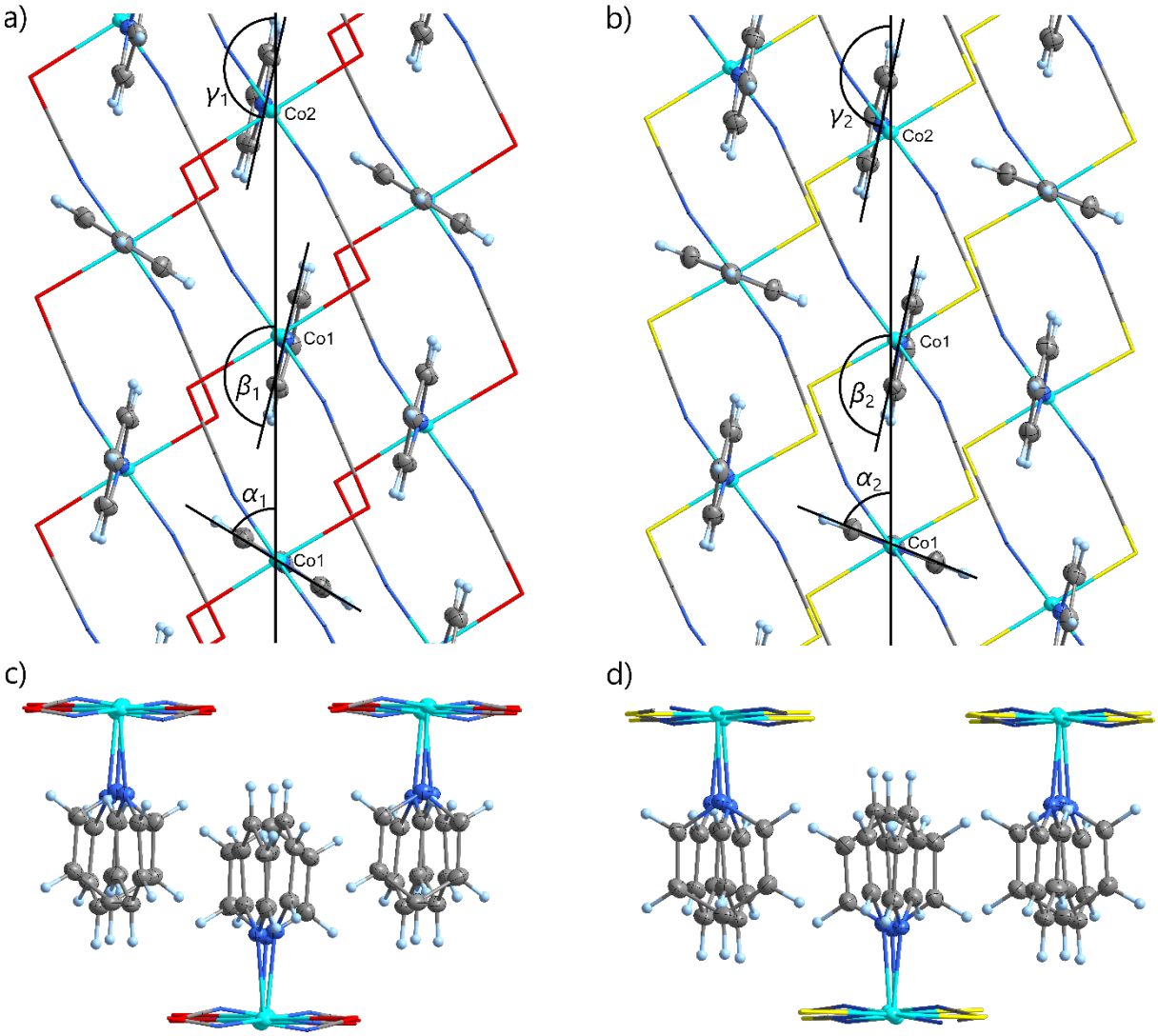

Figure S11. Influence of the orientation of the axial pyridine ligands at the cobalt(II) ions on the crystal packing of compound **1** (left) and **2** (right). Bottom: View along the chain direction. Top: View rotated by 90° with respect to the chain direction. The angles between the axial pyridine ligands and the chain axis (in °) are given for (i) the selenocyanate compound **1**: α_1 = 56.99(2) (Co1), β_1 = 165.43(2) (Co1), γ_1 = 165.43(2) (Co2); and (ii) the thiocyanate compound **2**: α_2 = 67.52(4) (Co1), β_2 = 168.31(3) (Co1), γ_2 = 167.99(4) (Co2).

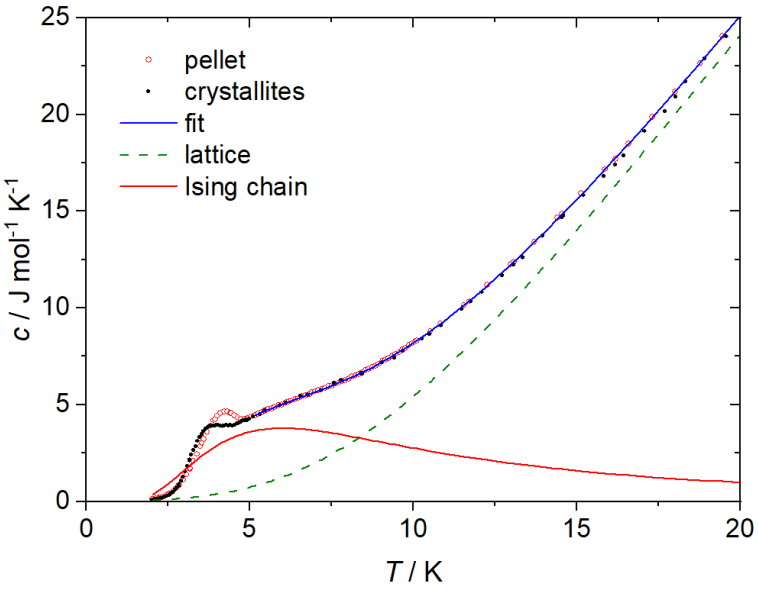

Figure S12. Heat capacity $c(T)$ of compound **2** measured using two samples from the same batch. One sample was pressed into a pellet by temporarily applying a pressure of approximately 1000 bar (200 kg on 5 mm diameter pellet) (red points), while the second sample consisted of crystallites sprinkled onto the microcalorimeter (black points). The mass of the non-pressed sample was determined using scaling the specific heat at 10 K. The influence of sample handling on the critical temperature of magnetic ordering is evident: the non-pressed sample exhibits a maximum in $c(T)$ at 3.9 K, whereas pressing shifts this maximum to 4.25 K. The solid blue line represents a fit to the data in the temperature range 5–20 K, consisting of the sum of the lattice contribution (dashed line) and the Ising spin-chain contribution (red line). The lattice contribution was modeled as a linear combination of Debye and Einstein phonon contributions. Fit parameters: Debye temperature T_D = 85(2) K, Einstein temperature T_E = 136(9) K, exchange coupling J_{Ising}/k_B = 29.2(2) K (20.3(1) cm^{-1}), based on the Hamiltonian $-J_{Ising} \Sigma_n S^z_n S^z_{n+1}$ for an effective ground-state doublet spin $S = 1/2$.

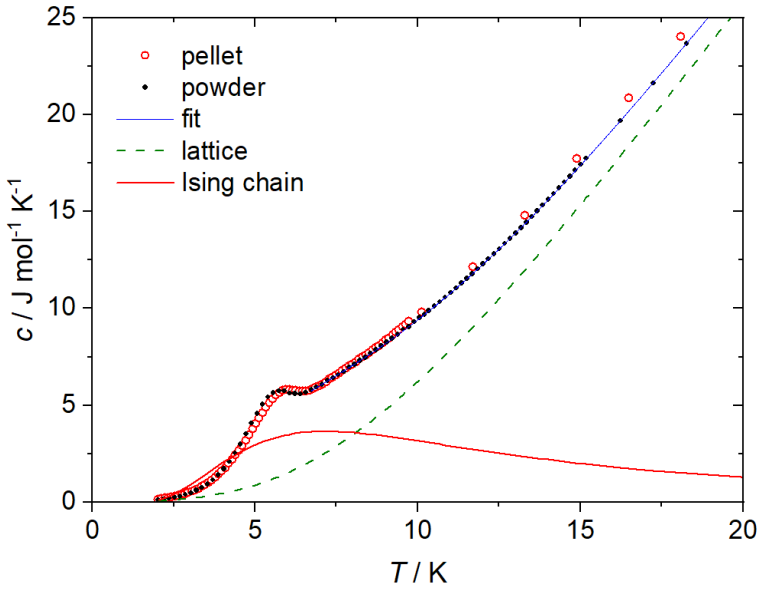

Figure S13. Heat capacity $c(T)$ of two batches of compound **1**. One sample was pressed into a pellet by temporarily applying 1000 bar (red points), while the second sample consists of compacted powder prepared under a pressure of approximately 50 bar (black points). The influence of sample handling on the critical temperature of magnetic ordering is evident: the powder sample exhibits a maximum in $c(T)$ at 5.8 K, whereas pressing shifts this maximum to 6.0 K. The solid blue line represents a fit to the data in the temperature range 7–20 K, consisting of the sum of the lattice contribution (dashed line) and the Ising spin-chain contribution (red line). Fit parameters: T_D = 74(1) K, T_E = 115(2) K, and J_{Ising}/k_B = 34.4(4) K (23.9 cm^{-1}), for details see Figure S12.

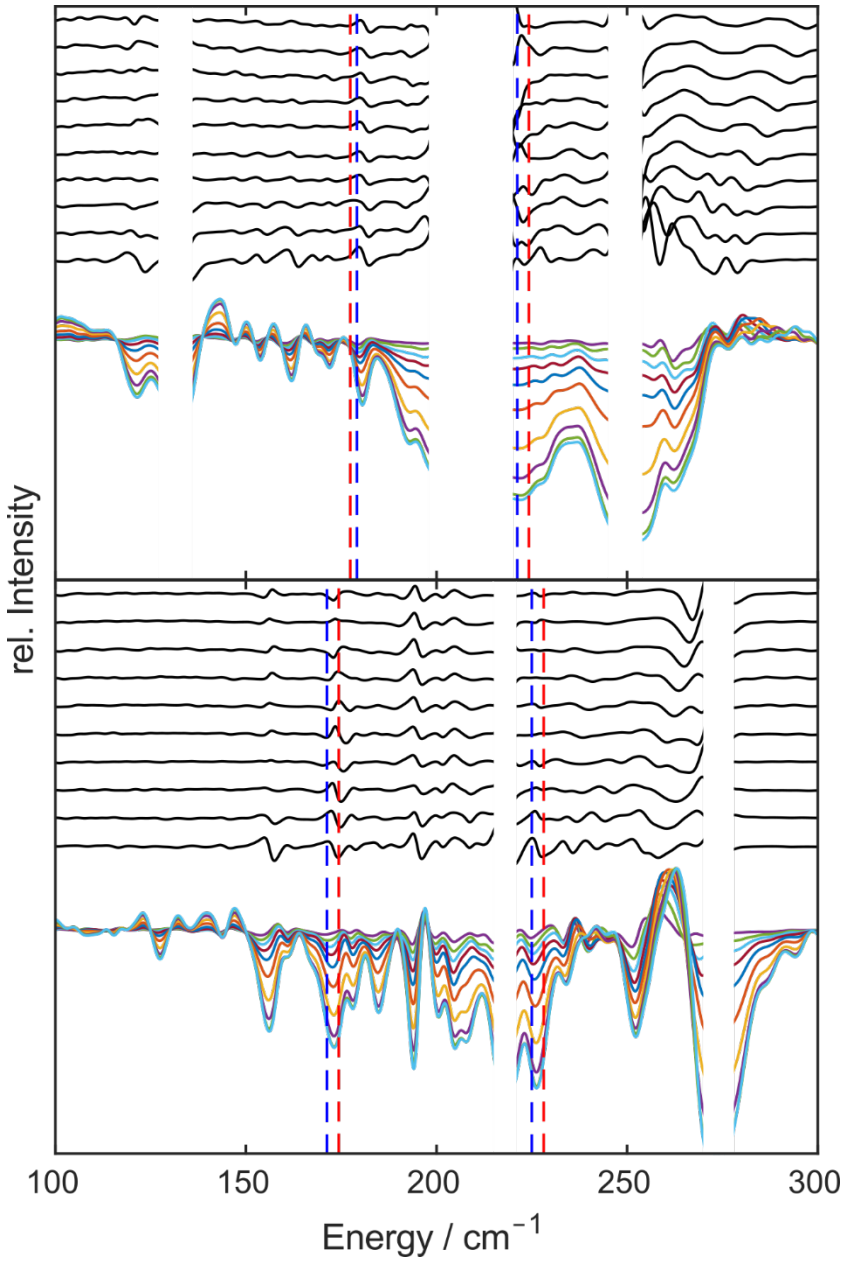

Figure S14. Magnetic-field dependence of the THz-EPR spectra of **1** (top) and **2** (bottom) measured at 5 K. The black solid lines represent magnetic-field division spectra (MDS), obtained by dividing a raw spectrum recorded at (B_0+1) T by that measured at B_0, with B_0 ranging from 0 T (bottom trace) to 9 T (top trace). The colored spectra at the bottom show the corresponding magnetic-field subtraction spectra (MSS) of **1** and **2**, respectively. The red dashed lines indicate the zero-field transition energies calculated from ab initio methods. For clarity, blank white regions were manually inserted to mask spectral regions with low transmittance and consequently high numerical noise. The assigned transitions are highlighted by blue dashed lines.

Table S4. Relative energies for all quartet and the twelve lowest doublet states obtained from ab initio CASSCF and CASPT2 calculations for **1** and **2** (see Figure S1 for depiction of the structural models)

2*S*+1	Term	**1**-Co1		**1**-Co2		**2**-Co1		**2**-Co2	
		CASSCF	CASPT2	CASSCF	CASPT2	CASSCF	CASPT2	CASSCF	CASPT2
4	^{4}F	0	0	0	0	0	0	0	0
		253	384	501	546	155	276	489	532
		973	1131	1069	1073	906	931	1035	919
		5403	6441	5402	6262	5606	6669	5566	6454
		7720	8717	7951	8765	7819	8921	8057	8992
		8758	9711	8871	9640	8710	9758	8777	9638
		15615	17485	15828	17558	15824	17868	15932	17849
	^{4}P	21010	19117	21151	19137	21120	18768	21195	18722
		22320	20819	22257	20586	22337	20397	22334	20246
		25806	23862	26462	24454	25861	23596	26409	24077
2	^{2}G+^{2}P	11727	9377	11517	8994	11584	9076	11529	8879
		15678	13092	16067	13384	15512	12809	15969	13182
		17539	16101	17358	15736	17642	15784	17570	15550
		18433	16850	18183	16446	18403	16422	18208	16106
		19163	17597	19099	17353	19059	16586	19085	16467
		19718	17800	20040	18021	19768	17052	20093	17272
		20695	18871	20861	18924	20642	17955	20840	18060
		21241	19304	21302	19238	21225	18360	21336	18377
		24132	21649	24150	21632	24165	20733	24202	20722
		24450	22568	24346	22325	24492	21560	24459	21418
		24645	23871	24773	23869	24791	23147	24887	23080
		24916	21973	24942	21862	24890	21097	24968	21053

Table S5. Relative RASSI-SO energies (in cm^{-1}) of the six lowest Kramers doublets of the $^4T_{1g}$ ground multiplet for the two crystallographically independent cobalt(II) centers in **1** and **2** (see Figure S1 for depiction of the structural models)

term	subterm	KD	**1**-Co1	**1**-Co2	**2**-Co1	**2**-Co2
^4F	$^4T_{1g}$	1	0	0	0	0
		2	224	177	228	174
		3	595	720	547	722
		4	893	967	847	969
		5	1508	1425	1363	1318
		6	1580	1502	1439	1407

Table S6. Cartesian *g*-tensor components (S_{eff} = ½) for the first two Kramers doublets of Co1 and Co2 in **1** and **2**, as obtained from ab initio calculations (see Figure S1 for depiction of the structural models)

		1-Co1	**1**-Co2	**2**-Co1	**2**-Co2
KD1	E_{KD1} (cm^{-1})	0	0	0	0
	g_x	1.613	1.773	1.898	2.047
	g_y	1.982	2.648	2.365	4.012
	g_z	8.181	7.587	7.864	6.483
KD2	E_{KD2} (cm^{-1})	224	177	228	174
	g_x	2.204	2.089	1.860	1.014
	g_y	2.912	2.190	2.640	1.221
	g_z	4.325	5.239	4.418	5.451

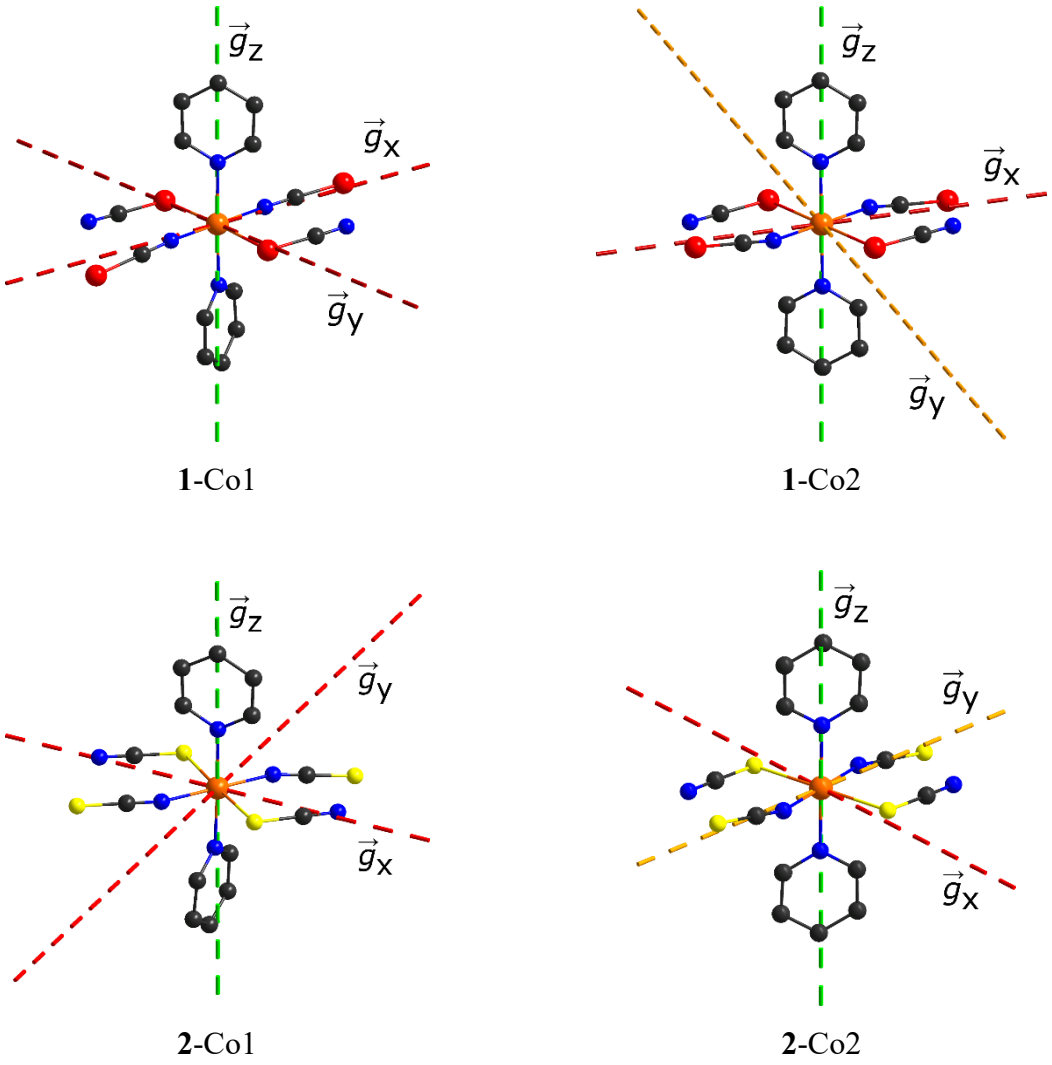

Figure S15. Representation of the magnetic axes of the ground state Kramers doublet (S_{eff} = ½) as obtained from ab initio calculations on the mononuclear model structures of **1** and **2**. Color code: green, easy axis of magnetization (g_z); orange, intermediate axis of magnetization (g_y); red, hard axis of magnetization (g_x).

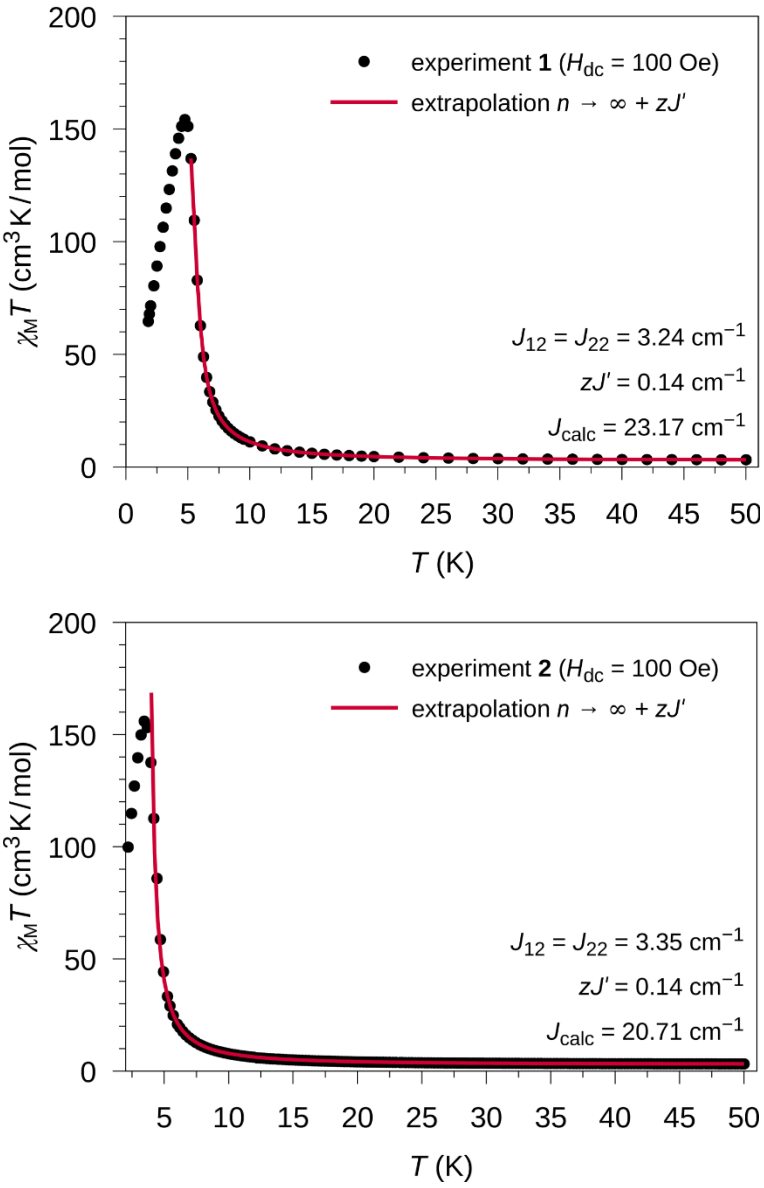

Figure S16. Temperature dependence of the experimental $\chi_M T$ data (•) for **1** (top) and **2** (bottom) measured under an applied dc field of 100 Oe. The solid red lines represent a fit of the magnetic susceptibility based on the single-ion parameters using an *n*-membered spin-ring coupling scheme extrapolated to $n \rightarrow \infty$ with mean-field correction.

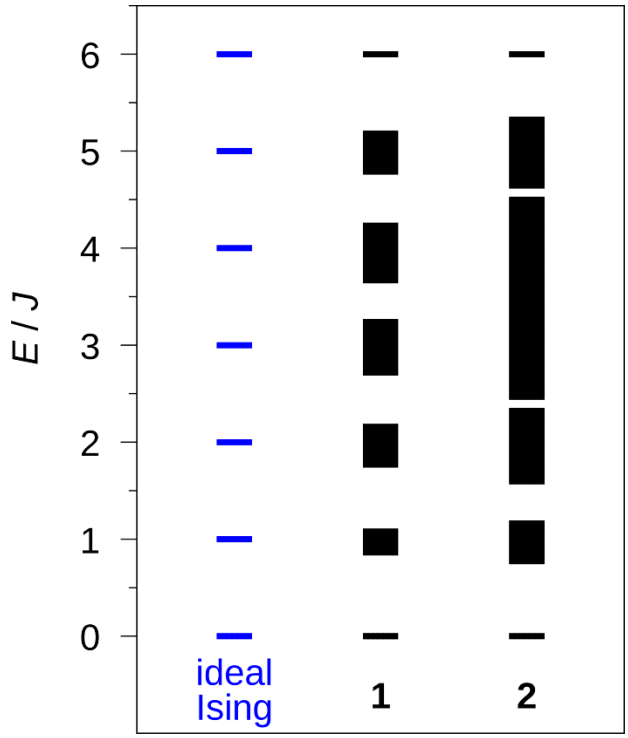

Figure S17. Energy-level scheme of spin states expressed in units of the idealized Ising coupling constant *J*, as obtained from POLY_ANISO calculations within the OpenMolcas package of programs using the results of the ab initio calculations of the mononuclear structural models of **1** and **2** (black). For both simulations, a 12-membered spin-ring coupling scheme together with the coupling constant extracted from the Lines model (**1**: J_{Lines} = 3.24 cm^{-1}; **2**: J_{Lines} = 3.35 cm^{-1}) were employed. The spin states depicted in blue represent the expected multiplet splitting for an ideal Ising anisotropy.